南京航空航天大学

论文集

（二〇〇〇年）

第13期

南京航空航天大学科技部编

二〇〇一年六月

四　　院

○四一系

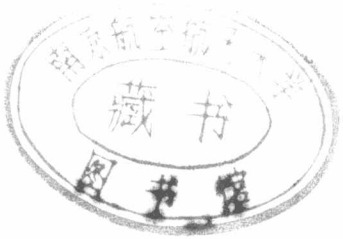

目 录

序号	姓名	职称	单位	论文题目	刊物、会议名称	年、卷、期	类别
363	朱岱寅 Rolf Scheiber 朱兆达	讲师	041	Impacts of an efficient topography adaptive filter on coherence estimation and phase unwrapping	Proc. Of EUSAR 2000	2000	
364	关振红	硕士	041	基于 APAC517 实现高速实时数据显示	空载雷达	000003	
365	关振红 郑启生 朱兆达	硕士	041	基于 SHARC-ADSP21060 实现高速转角变换	气象仪器装备	000004	
366	宋茂忠	副教授	041	GPS 多径误差特性与抗多径方法	南京航空航天大学学报	9931 增	J*
367	宋茂忠	副教授	041	用信息理论模型来研究教学过程	南京航空航天大学学报（社会科学版）	0002 增	
368	宋茂忠	副教授	041	用加权几何精度因子选星的 GPS 抗多径定位方法	南京航空航天大学学报	003205	J
369	潘永东 王小扬 王金香	硕士	041	基于神经网络的 ICAI 软件的设计与实现	南京航空航天大学学报	003201	J
370	杨建华 赵 力	硕士	041	基于VQ与HMM相结合的汉语数字语音识别	南京航空航天大学学报（英文版）	001701	J
371	王成华 吕 勇	副教授	041	8031 芯片主要模块的 VHDL 描述与仿真	航空电子技术	000004	H
372	王成华 包 骅	副教授	041	Research on Nonlinear Distortion in Amplifiers	南京航空航天大学学报（英文版）	003202	J
373	吴 宁 张兴敢	副教授	041	用选通门匹配方法提高计算式频率计的测量精度	数据采集与处理	001501	H
374	吴 宁	副教授	041	基于组合逻辑的复模准浮点计算方法	航空电子技术	000002	H
375	郑步生	讲师	041	电子设计自动化实验环境的建设与管理	实验室研究与探索	000005	J
376	郑步生 蒋 璇	讲师	041	EDA 技术的发展对电类专业教学的影响及应对策略	南京航空航天大学学报（社科版）	000203	
377	顾长青 舒永泽 徐金平	副教授	041	A subdomains Splicing Technique for IPO Approach	第五届国际天线、电波传播与电磁理论学术会议	2000	
378	周永刚	助教	041	半导体激光器的发展简述	科技信息	000003	
379	仰枫帆 梁树雄 毕光国	博士后	041	移动通信DS/SSMA系统相位扩频谱序列的设计准则	IEEE Six international sympposium on spread spectrum Techniques and Applications	2000	
380	周建江	博士后	041	在教学中把能力培养落到实处	南京航空航天大学学报（社科版）	000200	
381	Y. F. Li 黎 宁	讲师	041	Development of a physically behaved robot work cell in VR for task teaching	Robotics and computer Integrated Manufacturing	001600	H*
382	黎 宁 Y. F. Li	讲师	041	Methed for image segmentation based on an encoder-segmented neural network and its application	Optical Engineering	993805	H*

Proc. of EUSAR 2000

IMPACTS OF AN EFFICIENT TOPOGRAPHY ADAPTIVE FILTER ON COHERENCE ESTIMATION AND PHASE UNWRAPPING

Daiyin Zhu[*], *Rolf Scheiber*[**], *Zhaoda Zhu*[*]

[*] Department of Electronic Engineering, Nanjing University of Aeronautics and Astronautics, 210016 Nanjing, China,
Tel: ++86 25 4892410, Fax: ++86 25 4498069, E-mail: njydfz@jlonline.com

[**] Deutsches Zentrum für Luft- und Raumfahrt (DLR) e.V.
E-mail: Rolf.Scheiber@dlr.de

ABSTRACT

In this work, an efficient implementation of the topography adaptive filter based on local frequency estimation is proposed, where chirp-z transform is applied to enhance the accuracy of the frequency estimation. As a by-product of this adaptive filter, the linear approximated phase model of the interferogram is employed to improve the coherence estimation. The impacts of the adaptive filter on global and local phase unwrapping algorithms are discussed. Finally, aiming at the negative effect that the adaptive filter can bring to local phase unwrapping algorithms, a fusion scheme that takes advantage of least square and several local phase unwrapping algorithms is presented.

1 INTRODUCTION

Interferometric SAR (InSAR) is powerful in digital topography modeling, even though, the thermal noise, spatial and temporal decorrelation noise, which make the interferogram quite noisy, always encumber us from deriving as much as possible the terrain characteristic from the two complex SAR images acquired from different orbits. To filter the interferogram is one of the crucial steps in the InSAR signal processing routine, without which it is almost impossible to unwrap the phase correctly, and hence to reconstruct the topography. The purpose of the filtering of the interferogram is to reduce the phase noise and "repair" phase fringes. The interferometric phase that has been wrapped into the interval of $[-\pi,+\pi)$ should be considered as a random process, and is supposed to be stationary in a small area although it is not true in the large extent of the interferogram. To filter the interferogram with a moving box is called "multilook", it is the maximum likelihood estimator of the interferometric phase originating from constant terrain after the flat earth phase is removed. With an appropriate number of "looks", we can reduce the phase noise, and improve the contrast of the interferometric phase map as well. The so-called "multilook filter" is essentially a 2-D low pass filter, it eliminates the signal in case of steep topography as well as suppresses noise in the stop band. So, the multilook filter will smear the tight fringes of the interferometric phase map, and also cause underestimation at the precipitous terrain. We try to overcome this defect of the multilook filter by a local frequency estimation technique, which will center the pass band of the 2-D filter on the maximum magnitude of the 2-D local Fourier spectrum of the interferogram. Local frequency estimation makes the pass-band of the filter track the variation of the topography, in other words, it introduces a topography adaptive filter.

In the recent literature, there are diverse schemes to implement the filtering of the interferogram by local frequency estimation techniques. For example, the schemes in [1], [2], [3] are based on the MUSIC algorithm, 2-D FFT, and Energy Separation Algorithm, respectively. In this paper, we propose a scheme based on the chirp-z transform in section 2. During the implementation of the filtering scheme the linear approximated phase model of the interferogram is extracted as a by-product, which can help to improve the coherence estimation, and hence provides a more reasonable quality map for phase unwrapping. In section 3 and 4, the impacts brought by this topography adaptive filter on coherence estimation and phase unwrapping algorithms are analyzed respectively. To remove the negative effect caused by this adaptive filter on the local phase unwrapping algorithms, in section 5, a phase unwrapping scheme based on the fusion of the least square and several local phase unwrapping algorithms is proposed. We use X-SAR data of the Mt. Etna and ERS data taken from the vicinity of Vienna as examples to study the performance of the filter.

2 THE TOPOGRAPHY ADAPTIVE FILTER

Two complex SAR images used for interferometry can be modeled as,

$$\begin{aligned} s_1 &= c + n_1 \\ s_2 &= c \cdot e^{-j\phi_T} + n_2 \end{aligned} \tag{1}$$

Here, c is the common part in the two SAR images, n_1 and n_2 are the decorrelation noise, c, n_1 and n_2 are assumed to be uncorrelated circular Gaussian random processes, and ϕ_T is the phase caused by the topography. We use the conjugate multiplication to form the interferogram,

$$I = |c|^2 \cdot e^{j\phi_T} + c \cdot n_2^* + c^* \cdot n_1 \cdot e^{j\phi_T} + n_1 \cdot n_2^* \tag{2}$$

I is non-stationary because of the term $|c|^2 \cdot e^{j\phi_T}$, whereas the remaining three terms are stationary in a wide sense. Strictly speaking, it is not reasonable to do moving average over the interferogram because of its non-stationarity, especially in conditions that the terrain is very precipitous. In such areas, even the rough assumption, that I is stationary in a small window is no longer correct, and the moving average that ignores this point will smear the fringes. The first term of (2) can be decomposed as:

$$e^{j\phi_r} \cdot |c|^2 \cdot e^{j(\phi_T - \phi_r)} \tag{3}$$

where ϕ_r is the coarse topography phase, and $|c|^2 \cdot e^{j(\phi_T - \phi_r)}$ stands for the detail of the topography. If we are able to extract the coarse topography phase from the interferogram, then (2) is rewritten as,

$$\begin{aligned} I = e^{j\phi_r} \cdot [&|c|^2 \cdot e^{j(\phi_T - \phi_r)} + c \cdot n_2^* \cdot e^{-j\phi_r} \\ &+ c^* \cdot n_1 \cdot e^{j(\phi_T - \phi_r)} + n_1 \cdot n_2^* \cdot e^{-j\phi_r}] \end{aligned} \tag{4}$$

The detail of the topography, i.e. the term $|c|^2 \cdot e^{j(\phi_T - \phi_r)}$ is the mean of the stationary process in the brackets of (4). We can achieve the maximum likelihood estimation (MLE) of it by moving average under the assumption of ergodicity. The extraction of the coarse topography can be accomplished by fringe detection. In our filtering scheme, this goal is achieved by generating a linear approximated interferometric phase model.

2.1 STRUCTURE OF THE TOPOGRAPHY ADAPTIVE FILTER

The topography adaptive filter is a linear system, and it should be expressed in the spatial domain as,

$$\left\{\left[I(j,k) \cdot \left(h_{estimated\ fringe}(j,k)\right)^*\right] \otimes h_{moving\ box}(j,k)\right\} \cdot h_{estimated\ fringe}(j,k) \tag{5}$$

where $h_{moving\ box}(j,k)$ is the impulse response function of a moving boxcar filter, and $h_{estimated\ fringe}(j,k)$ is the estimated linear phase model, which stands for the coarse topography phase. $\otimes$ denotes the two dimensional convolution. The term $h_{estimated\ fringe}(j,k)$ plays the key role in the above filter, and is determined by the input interferogram through local fringe detection. If interpreted from the viewpoint of a band pass filter, it is the linear approximated phase model that provides information on the location of the center of the local interferogram spectrum, and hence guides us to design the band pass filter.

2.2 IMPLEMENTATION OF THE FILTER

The most noticeable feature of the interferometric phase map is its fringe pattern. If we separate a fairly small part of this interferogram, it should be possible to approximate its phase map with a plane. The spatial frequency of this two-dimensional linear phase can be estimated from the small separated interferogram by several methods. While estimating the frequency with 2-D FFT, the spectrum must be interpolated to improve the accuracy of the estimation. Computational complexity will be reduced if we only make interpolation in the main lobe of the spectrum. A 2-D FFT of the original size on the separated interferogram will bring us a coarse spectrum, then after its main lobe is located, only interpolation within this main lobe is needed to get a precise estimation of the local frequency. Chirp-z transform, which allows us to only achieve very high frequency sampling rate in a small interval on the unit circle, is employed to compute the discrete Fourier Transform within a small frequency interval [4].

The estimated phase plane is described as:

$$\varphi(f_j, f_k) = e^{j2\pi(f_j \cdot j + f_k \cdot k)} \cdot e^{j\phi_0} \tag{6}$$

where f_j, f_k are the maximum likelihood estimates of the 2-D spatial frequency components, and ϕ_0 is the initial phase. $e^{j\phi_0}$ is computed as the normalized complex average of the separated interferogram after the linear phase is removed from it.

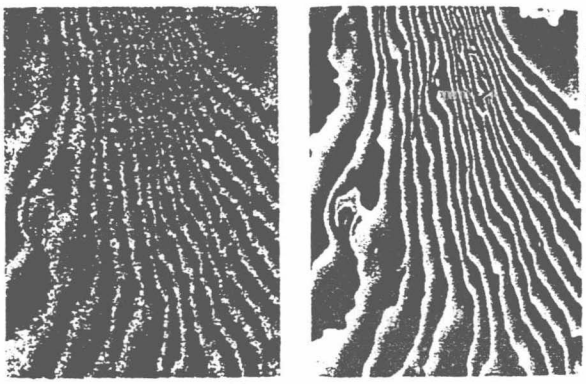

(a) (b)

Figure 1: *Interferometric phase (a) and linear approximated phase model (b) of X-SAR Mt. Etna data*

At the same time that we get the coarse 2-D Fourier spectrum of a separated interferogram, the local SNR can be evaluated by the ratio between the magnitudes of the main lobe and side lobe of the spectrum. The local SNR is also a scale of the confidence of the frequency estimation. If the local SNR is smaller than a given threshold, we enlarge the estimation window to twice of its original size for more reliable estimation results and calculate the local SNR again. If the new SNR is still lower than the threshold, a mandatory spatial frequency of 0 is set. The mandatory frequency is usually assigned to areas that are totally decorrelated (e.g. water, high vegetation in repeat-pass InSAR).

We go through the whole interferogram by 50 percent overlapping the estimation window, then taper weighting the estimated 2-D linear phasor, after that reassembling them by superposition [5] to get $h_{estimated\ fringe}(j,k)$, i.e. the linear approximated phase model. Because the computational efficiency of making maximum likelihood estimation on the phase of each pixel is not acceptable, the

overlapping can also be considered as an interpolation scheme, which avoids estimating the dominant 2-D frequency point by point over the whole map. An example of the performance of this filtering scheme is presented in Fig. 1. The input interferometric phase and the linear approximated phase model extracted from X-SAR Mt. Etna data are shown in (a) and (b) respectively..

The local SNRs will also be combined after taper weighting to get an SNR map of the interferogram, which can also be used as an additional quality map for phase unwrapping.

3 IMPACTS OF THE LINEAR PHASE MODEL ON COHERENCE ESTIMATION

We improve the coherence estimation by identifying the topography term with the linear approximated phase model $h_{estimated\ fringe}$. It should be removed from the interferogram prior to the estimation of the coherence over a large window. Thus the product of thermal and temporal decorrelation $\gamma_{thermal} \cdot \gamma_{temporal}$ should be estimated as,

$$\gamma_{thermal} \cdot \gamma_{temporal} = \frac{\left| \sum_{j,k \in w} s_1 \cdot s_2^* \cdot h^*_{estimated\ fringe} \right|}{\sqrt{\sum_{j,k \in w} |s_1|^2 \cdot \sum_{j,k \in w} |s_2|^2}} \qquad (7)$$

Additionally, the linear approximated phase model can also be used for the spatially adaptive implementation of the spectral shift filter as proposed in [6].

4 IMPACTS OF THE ADAPTIVE FILTER ON PHASE UNWRAPPING

The performance of the filtering scheme should be investigated with respect to its impacts on phase unwrapping. In general the adaptive filter should facilitate phase unwrapping, but sometimes it also has negative effects because of the artificial fringes caused by the noise corrupted frequency estimation. In this section, we will study the impacts of the adaptive filter on the global and local phase unwrapping algorithms and put emphasis on the negative effect in the case of local methods from the perspective of residue distribution.

4.1 IMPACTS ON THE LEAST SQUARE PHASE UNWRAPPING METHOD

As is well known [7], phase noise induces slope under estimation for least square phase unwrapping algorithms. Therefore filtering must be proceeded prior to least square phase unwrapping methods. It is well known [1-3] that a topography adaptive filter performs better than the conventional multilook filter. Nevertheless, the need for weighting/masking particular areas cannot be overcome in general. The generation of the adequate weights is not necessarily solved by the proposed topography adaptive filter, but the performance of least square methods is generally improved.

4.2 IMPACTS ON THE LOCAL PHASE UNWRAPPING METHODS

If the phase unwrapping problem is not singular, there is definitely a reasonable or correct way to define the integral path for local phase unwrapping methods, along which unwrapping errors will be localized. Nevertheless, our capability of defining it is problematic; in case of high residue density the correct way is usually unavailable and the robustness of any of the local algorithms will be destroyed due to the high level of phase noise.

To compensate the shortness of our ability to find the right integral path in noisy phase maps, filtering of the interferogram is still necessary as a preprocessing step of local algorithms. Despite that the topography adaptive filter can greatly reduce the residue density, sometimes it also has negative effect on the local algorithms. This is caused by the artificial fringes generated by the filter in the situation of low coherence. The artificial fringes that make difficulties for phase unwrapping do not come from topography, but from noise.

For some certain residue distributions like dipoles and near distance residue pairs it is very easy to define a reasonable integral path, while for isolated residues it becomes quite difficult. From the perspective of residue distribution, the artificial fringes generated by the local frequency estimator in low coherence areas often bring us residue pairs with farther distance and even isolated residues. Artificial fringes do not tend to make the phase unwrapping problem singular, but as the distance between residues is enlarged, to connect residues with opposite charges sometimes does become more difficult.

The linear approximated phase model $h_{estimated\ fringe}(j,k)$ in the filtering scheme is normally not rotation free. After it has been subtracted from the input interferogram, the residue map of the residual phase, which is expressed as the principal phase value of the term in the brackets of Equation (4) must be different from that of the input interferogram. The residue pairs with farther distance and isolated residues caused by artificial fringes will also appear in the residue map of the residual phase. The residual phase will be multilooked afterwards, but the adverse residue distribution can still remain even after being smoothed. Next, to finish the filtering process, the smoothed residual phase has to be added back to the linear approximated phase model. In this step, two phase maps both with artificial residues, will be superimposed to each other and there is no guarantee that these artificial residues will cancel out or form near distance residue pairs. To overcome these problems we propose the following fusion scheme.

5 A FUSION SCHEME FOR PHASE UNWRAPPING

In order to adapt the filtering scheme to path following methods, we propose a modified version of the adaptive

filter. As is well known, least square methods can give a smooth result, so our intention is to modify $h_{estimated\ fringe}$ through unwrapping it with the unweighted least square estimator. In this way, usually a residue free phase field can be obtained. After subtracting it from the input interferogram we get a residual phase map, which has nearly the same residue distribution as the input interferogram. To unwrap the residual phase map by any path following method is as difficult or as easy as to directly unwrap the phase map of the input interferogram because of the same residue map they have. Before smoothing the residual phase to reduce the phase noise, the artificial residues do not occur and after the smoothed residual phase is added back to the unwrapped linear approximated phase model, still no artificial residues are introduced.

Our fusion scheme for phase unwrapping is described next: First the modified adaptive filtering scheme is proceeded; Then for phase unwrapping, we first generate the mask cuts with the mask cut algorithm [8], and then unwrap the smoothed residual phase. During the unwrapping process a binary map is generated, which is a flag on each pixel and indicates if it has been unwrapped or not. Then the areas marked as wrapped are unwrapped with a region growing algorithm. For the region growing algorithm, pseudo-correlation is utilized as a quality map. Pseudo-correlation can point out the position of residues very precisely, and the integral path of region growing will be guided in a more appropriate manner. Besides the pseudo-correlation, the SNR map is also used to set a lower limit to stop the region growing. The reason why two different quality maps are used here is just for the improvement of the robustness. An example of phase unwrapping using the fusion scheme is presented in Fig 2.

6 SUMMARY

An efficient implementation of the topography adaptive filter based on the chirp-z transform has been presented and its benefits for coherence estimation have been explained. With respect to phase unwrapping its potential to repair fringes was shown, but sometimes it also induces broken or lost fringes because of the artificial fringes caused by the corrupted frequency estimation. Therefore the adaptive filter incorporated with the least square estimator is suggested prior to using the local phase unwrapping algorithms.

7 ACKNOWLEDGEMENT

The work presented in this paper was performed within a collaboration of the Chinese Aeronautical Establishment (CAE) and the German Aerospace Center (DLR).

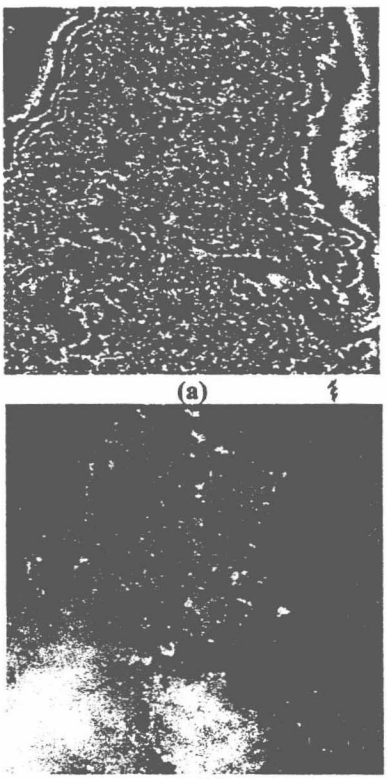

Figure 2: *Result of phase unwrapping using the fusion scheme, (a) wrapped phase map, (b) unwrapped phase*

8 REFERENCES

[1] E. Trouve, J. Nicolas, and H. Maitre, "Improving phase unwrapping Techniques by the use of local frequency estimation", IEEE Trans. Geosci. Remote Sensing, vol.36, pp.1963-1972, November 1998.

[2] M. Hubig, "A maximum likelihood a priori filter for interferometric phase", Proceedings of IGARSS'99

[3] D. Perea-Vega and I. Cumming, "Local frequency Estimation in interferograms using a multiband prefiltering approach", ESA-Fringe workshop'99

[4] A.V. Oppenheim, R.W. Schafer: "Discrete Time Signal Analysis", Prentice Hall, London, 1999

[5] R. Goldstein and C. Werner, "Radar ice motion interferometry", Proc. 3rd ERS symp. on Space at the service of our Environment, Florence, Italy, March 1997

[6] G.W. Davidson and R. Bamler: "Multiresolution phase unwrapping for SAR interferometry", IEEE Trans. Geosci. Remote Sensing, vol.37, pp.163-174, Jan, 1999.

[7] R. Bamler, N. Adam, G. W. Davidson, and G. Just, "Noise-induced slope distortion in 2-D phase unwrapping by linear estimators with application to SAR interferometry", IEEE Trans. Geosci. Remote Sensing, vol.36, pp.913-921, May, 1998.

[8] J. Flynn, "Consistent 2-D phase unwrapping guided by a quality map", Proceedings of IGARSS'96

基于 APAC517 实现高速实时数据显示*

关振红

（南京航空航天大学 264 信箱）

[摘要] 本文介绍了用于信号和数据处理的 ADSP-2106X SHARC 多机系统中实现实时图像显示的一种方法，并以某型雷达信号处理机数据显示为实例，讨论了使用 APAC517 过程中的一些关键问题。

关键词 实时信号处理 SHARC APAC517 数据显示 雷达

1 引 言

APAC517 是功能强大的彩色显示模块并且能使用在标准的 SHARCPAC 多处理器环境中。它非常适合运用于以 ADSP-2106X SHARC 系列处理器为核心的信号处理系统中。APAC517 主要由一个 120MFlops ADSP-2106X SHARC（以下简称为 SHARC）处理器及一些外围电路组成。APAC517 主要性能如下：

• SHARC 具有 512K×48 位零等待静态缓冲区 SRAM；

• 2MBytes 的显示缓冲区 VRAM 分成两个区，支持真彩色和伪彩色方式；

• 24 位真彩色方式下，APAC517 能提供 512×512 显示分辨率；

• 8 位伪彩色方式下，APAC517 能提供 1024×1024 显示分辨率；

• APAC517 能提供 256K×16 大小覆盖显示缓存 Overlay RAM；

• APAC517 具有 SHARCPAC 的所有功能，包括标志、中断、串口、JTAG 等等。

该模块以SHARC为核心进行图像显

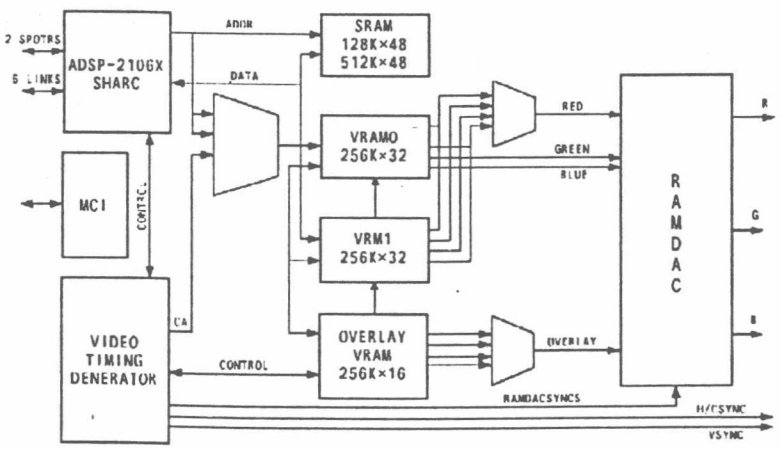

图 1 APAC517 拓扑结构图

• 本文于 2000 年 6 月 8 日收到。

示，而 SHARC 有多个数据通信口，包括 6 个 4 位高速 LINK 口（总传送速率为 240MBytes/s）及 2 个高速串口（总传送速率为 80Mbit/s），这样 APAC517 可以方便地用于 SHARC 多机系统。图 1 是 APAC517 结构图。

2 APAC517 主要工作原理

2.1 扫描方式

APAC517 支持多种显示格式，常用的有：640×480 逐行扫描（VGA），800×600 逐行扫描（SVGA）及 1024×768 隔行扫描。如果用户需要特殊显示格式还可以自己开发。影响扫描方式的控制寄存器主要有：VTOTAL，确定一场或一帧中总共有多少个半行；VBLANK，确定场或帧消隐脉冲的宽度；HTOTAL，确定水平扫描线的象素时钟总数；HBLANK，确定水平消隐脉冲的结束时刻或宽度。

2.2 显示缓存 VRAM

在真彩色和伪彩色方式下，象素的位数不同，它们在 VRAM 中的存放也不相同。下面重点介绍一下系统中采用的 8 位伪彩色方式。伪彩色方式 VRAM 中每 32 位字由四个象素组成，最低 8 位显示在屏幕上四个象素的最左端，次低 8 位显示在屏幕上左边第二个象素，以此类推，表 1 是 32 位字的组成结构。

表 1 伪彩色方式显示字结构

31 24	23 16	15 8	7 0
PIX_D[7:0]	PIX_C[7:0]	PIX_B[7:0]	PIX_A[7:0]

APAC517 允许用户对四个象素中一个象素进行操作而不改变其他象素的值，这样可以方便用户改变显示数据。表 2 为伪彩色方式下 VRAM 基地址组成。

表 2 伪彩色方式 VRAM 基址安排

VRAM 缓冲器	位	基址偏移量	访问类型
缓冲器 0	Word	0x0000 0000	读/写
	PIX_A	0x0040 0000	只写
	PIX_B	0x0050 0000	只写
	PIX_C	0x0060 0000	只写
	PIX_D	0x0070 0000	只写
缓冲器 1	Word	0x0004 0000	读/写
	PIX_A	0x0044 0000	只写
	PIX_B	0x0054 0000	只写
	PIX_C	0x0064 0000	只写
	PIX_D	0x0074 0000	只写
覆 盖	Word	0x0008 0000	读/写

对于显示屏幕上一点，设其坐标为（x，y）（坐标原点在屏幕左上角），伪彩色方式下，象素地址和象素在显示字中位置可以由以下两式确定：

象素地址＝Buffer 基址＋（y×256）＋（x/4）

象素在显示字中位置＝（X&3）＊8

APAC517 覆盖显示 VRAM 每个 16 位字由 4 个象素组成，象素在屏幕上的显示位置与伪彩色相似，系统中通过覆盖显示缓冲区在屏幕上显示字符用来说明显示画面的特征。

2.3 工作过程

APAC517 通过片上 SHARC 与信号处理系统其它部分进行数据通信，SHARC 首先加载一种显示格式，然后通过 LINK 口或多道串口接收待显示的数据。SHARC 将数据依次放入显示 VRAM 两个区中的一个区中（如 Buffer 0 中），当一屏数据放完后，SHARC 启动显示数据操作，即通知 Video Timing Generator 产生显示数据所需的各种信号，如：控制总线信号，控制 VRAM 信号，象素加载信号，场频信号，行频信号。VRAM 在 VTG 控制下将显示数据送给

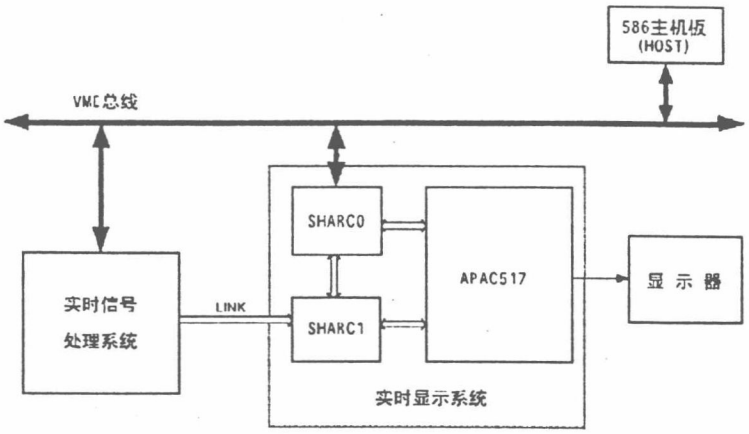

图 2 实时显示系统总体框图

RAMDAC 进行 D/A 变换，变换后的 R，G，B 信号连同 H/CSYNC 和 VSYNC 一同送往显示器。在 Buffer 0 数据进行显示的同时，SHARC 继续接收待显示的数据并将数据依次放入另一个缓冲区 Buffer 1 中，APAC517 的这种 VRAM 切换方式保证它能显示连续数据。

3 实时显示系统组成及工作过程

以下介绍的是某型雷达实际中采用的实时显示系统实例，该显示器由一块 APAC517 和两块 SHARC 及一些外围电路组成。图 2 是某型雷达信号处理系统的组成结构图。

实时信号处理系统在主机(HOST)的控制下，接收模拟信号进行实时信号处理，经处理系统处理过的数据通过 LINK 口向显示系统传送。显示系统中的 SHARC1 接收到数据后先进行数据取模、求整并合并 8 位象素，字符数据合并成 4 位数据；SHARC1 将象素数据通过 LINK 口送给 SHARC0 和 APAC517，SHARC0 将象素数据通过 VME 总线送给 HOST 进行二次处理，APAC517 接到数据后按照前述工作过

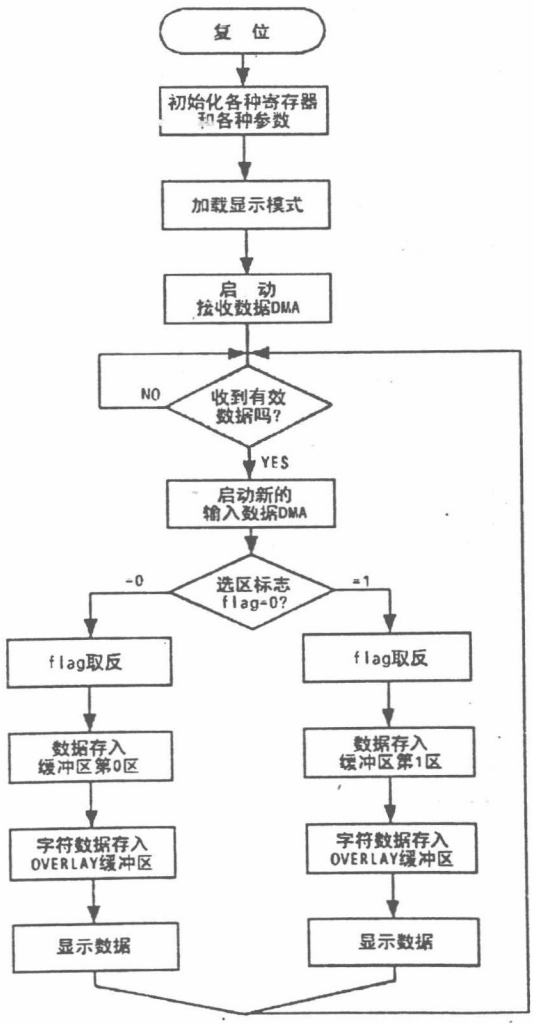

图 3 APAC517 的处理流程

程在显示器上进行显示。

本雷达显示系统采用 1024×695 逐行扫描方式，显示器的横向代表距离，纵向代表方向。显示系统在一帧数据中共接收 695 条距离线，每条距离线的长度为 1024。显示器行频为 24.30KHz、场频为 32.62KHz、象素时钟为 31.88MHz。图 3 是 APAC517 的处理流程。

4 测试结果

为了测试显示系统工作情况，在雷达信号处理系统输入端在一帧图像中输入 10 个点目标的线性调频信号，经过信号处理系统脉冲压缩处理后的数据送给显示系统。10 个点目标分布在等距离第 516 号方位线上，其它方位线没有回波。图 4 是在 APAC517 的 VRAM 一个区中回波信号的图形。图 5 是显示器显示的图像。

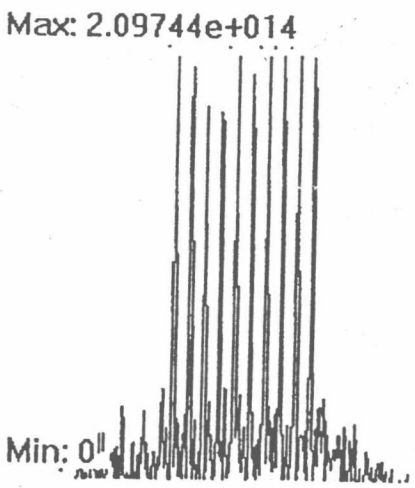

图 4 显示缓冲区中的数据

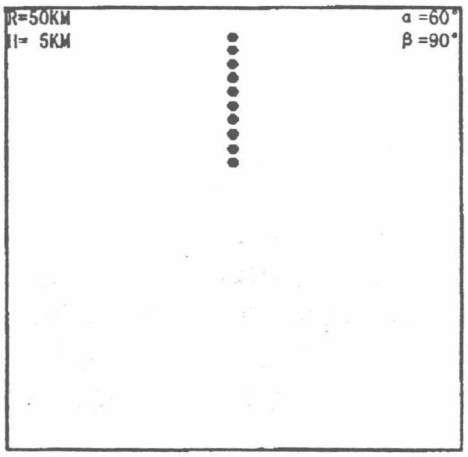

图 5 显示器显示结果

参 考 文 献

1 *AD* 公司，*ADSP-2106x SHARC User's Manual*，1995 年.

2 *SPECTRUM* 公司，*SHARC PAC-Video User Guide APAC*517，1998 年.

基于SHARC-ADSP21060实现高速转角

关振红

（解放军理工大学气象学院）

郑启生　　朱兆达

（航空工业总公司第607研究所）　（南京航空航天大学）

摘　要　本文以某型雷达信号处理机转角部分为基础，提出了一种新型实现实时矩阵转置方法，同时文中讨论多片SHARC-ADSP21060进行通讯的一些基本用法。

1　引　言

在某型雷达实时信号处理机的研制过程中，算法上要求信号处理机不仅对输入回波信号（已经AD变换）的距离向（横向）进行成像处理，还要对其方位向（纵向）进行成像处理，这就存在一个转角变换问题。实际研制的处理机选择了四片SHARC-ADSP21060（以下简称为SHARC）及两片大容量DRAM来实现的。

2　SHARC功能简介[1]

SHARC是指AD公司最新推出的超级哈佛结构处理器ADSP21060，这是目前世界上最先进的浮点处理器之一。

SHARC处理器的主要性能如下：

- 25ns指令周期；
- 80MFLOPS操作速度，峰值为120MFLOPS；
- 32位浮点或定点操作；
- 4Mbit内部RAM；
- 10个DMA通道，总传送速率为240MBytes/s；
- 外总线数据传送速率为240MBytes/s；
- 6个LINK口支持240MBytes/s的传送速率；
- 2个串行口支持80Mbits/s的传送速率；
- 寻址范围4G字。

SHARC除了运行速度高、高度并行操作、内部RAM容量大等特点外，其主要特点是数据通信口多。它有外总线接口和6个4位的高速LINK口及两个高速串行口。内部DMA控制器可支持10个DMA通道。

3　转角变换系统组成

实时信号处理机是以多片SHARC为核心设计的，转角变换也采用SHARC为核心

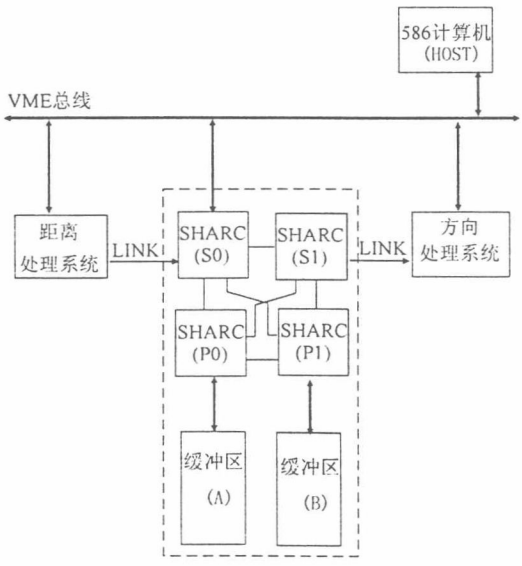

图1　转角变换系统组成图

的结构，这样便于系统之间数据传送。图1是转角变换系统拓扑结构。

从图中可以看出，转角变换系统由四片SHARC和两片各为8MBytes的大容量DRAM组成，S0和S1分别负责接收和发送数据。转角变换系统内部及转角变换系统和其它系统之间的数据通信通过LINK口以DMA[2]方式传送，LINK口之间的DMA传送速率为20MBytes/s。

4　转角变换系统工作原理

4.1　系统要求

处理机算法上要求从距离向抽取出的方位向数据帧与帧之间要有一定重叠，雷达正常工作时，转角变换系统连续接收数据，在一帧数据中共接收1898条周期为1 ms的距离数据线，每条距离数据线由2048(分成实部和虚部)个32位浮点数组成。每帧数据输出周期为1 ms的方位数据线1024条，每条方位数据线由4096个32位浮点数组成。

4.2　DRAM的划分

设P0控制的DRAM称为A区、P1控制的DRAM称为B区，它们的容量为8MBytes。一帧数据的容量为$2048\times2048\times32=8$Mbytes。每个区交替存放一帧数据。A区和B区分别分成两个子区，按照地址增加方向起的第一个子区称为子区1和子区2。子区1只能存储150条距离线，子区2可以存储1898条距离线，子区1所存储的150条距离线是用来实现方位向重叠的。图2是DRAM划分结构图。

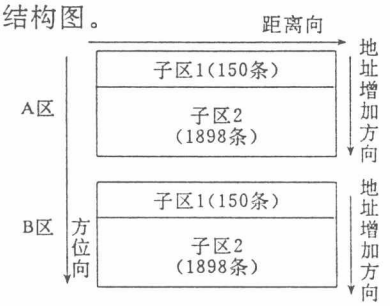

图2　外部缓冲区划分示意图

4.3　处理时间计算

处理机正常工作时，数据之间传递流水线不能破坏。从距离线抽取方位线时，要在一帧数据全部放在DRAM的一个区中才能进行抽取。由于输入数据线是连续变换的，因此要保证一个区放满数据前，另一个区数据抽取必须进行完成。输入1898－150＝1748条距离数据线的时间为1748×1 ms＝1.748s，抽取1024条方位数据线的时间为1024×1 ms＝1.024s。从时间上看，转角变换系统能正常工作。再来计算一下DMA时间，S0接收一条距离数据线到片内RAM的时间为$2048\times0.2=0.4096$ ms，从片内RAM到外部DRAM的时间为$2048\times0.025=0.0512$ ms，总时间为0.4608 ms，在输入周期为1 ms的时间内可以完成存数操作。同样道理，P0/P1从片外DRAM发送一条数据线到S1的时间为$4096\times0.025+4096\times0.2=0.9216$s，在输出周期为1 ms的时间内可以完成存数操作。

4.4　工作过程

S0从距离处理系统接收数据首先判断帧标志，如果帧标志为偶数，S0就把接收到的数据送给P0，是奇数就送给P1。P0接收到数据后，把数据按地址增加方向一条条地放入A区中。当一帧数据放满之后，P0启动数据抽取模块和1 ms定时器中断模块，P0将抽取的一条条数据线按1 ms的周期向S1发送。S1接收到P0的方位数据后直接向后一级方位处理系统发送数据。当P0进行帧标志为偶数的数据抽取时，S0将接收到帧标志为奇数的新一帧数据送给P1，P1也按照P0的过程进行操作。这样，距离数据实现连续写入，方位数据连续抽取，P0控制的A区和P1控制B区实现乒乓式读写。

5　测试结果

在转角变换系统调试过程中，在它的输入端按一定规律变化的数据，在输出端得到了预测的结果，但由于数据所占篇幅较大，此

处没列出。这里给出整个雷达正常工作时，信号处理系统连续接收到距离和方位频率都受调制的10个点目标回波信号。图3是距离处理结果，图4是方位处理结果。以上两副图证明转角变换是正确的，否则，方位向不能得到理想的处理结果。

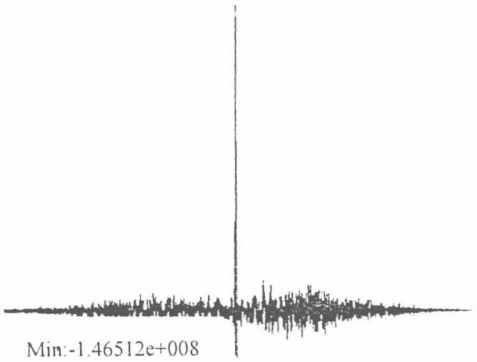

图3　距离处理结果

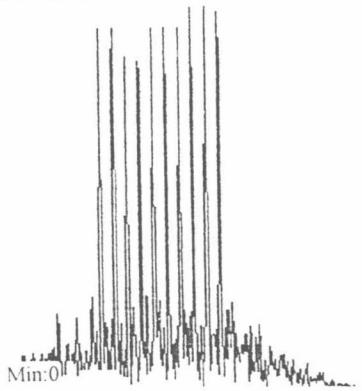

图4　方位处理结果

6 结　论

这种以SHARC为核心的转角变换系统比通常的用一片大容量的双端口RAM及一些计数器实现转角变换灵活、方便。以上只是介绍了转角变换系统的一种工作方式，实际上，由于雷达有多种工作状态，只要改变相应的SHARC的汇编程序就可以满足各种需要。这里介绍的转角变换系统特别适合使用SHARC为核心的信号处理系统中。

参考文献

[1] AD公司.《ADSP-2106x SHARC User's Manual》1995年

[2] SPECTRUM公司.《Wideband Computer Corporation 21K Optimized DSP Library Software License Agreement》1998年

（上接第27页）

$$\sum_{i=1}^{N=2}\delta_{\Phi i}=\delta_{\Phi 1}+\delta_{\Phi 2}=0.23+0.08=0.31\ (oe)$$

$$\beta_1=\frac{\sum_{i=1}^{N=3}\delta_{\Phi n_i}\times 360^\circ}{A_1}=\frac{0.31\times 360^\circ}{6000}=1'6''$$

3.7.5　方位同步轮系回差值

由于采用了弹簧双片齿轮，方位同步轮系回差值为零。

3.7.6　方位同步轮系总的精度

方位同步轮系总的精度计算值为1′6″。

已知：总体指标测量精度为0.1°，则方位传动传统的机械精度＝2′5″＋1′6″＝3′11″＜0.1°，满足总体指标要求。

3.8　俯仰传动比分配

3.8.1　驱动部分传动比按三级传动分配，传动比分别为6∶5∶6。

3.8.2　同步轮系分为粗同步和粗同步；粗同步传动比为1∶1，精同步传动比为36∶1。

3.9　天线座主轴减小晃动措施

天线座主轴上的承力轴承选用四点轴承，这样可避免通常使用的单列向心球轴承的径向间隙和轴向间隙，消除了主轴晃动，提高了雷达跟踪精度。

3.10　传动系统实测结果

方位传动系统回差实测值为$\beta_1=1'4''$(RMS)，

方位传动系统传动误差实测值为$\beta_2=1'1''$(RMS)，

实测验证值均达到产品设计计算要求。

第 31 卷增刊　　南京航空航天大学学报　　Vol. 31 Suppl.
1999 年 12 月　Journal of Nanjing University of Aeronautics & Astronautics　Dec. 1999

GPS 多径误差特性与抗多径方法*

宋茂忠
（南京航空航天大学电子工程系　南京，210016）

摘要　在近距差分 GPS(Global positioning system)等高精度定位中，多径干扰已变成了主要误差源。文中在分析多径干扰源分布的基础上，考虑了天线的多径抑制效应，建立了 GPS 接收机的伪码跟踪与载波同步复合环的等效数学模型，并分析了多径参数对伪距观测量的误差特性，给出了许多有用结果，最后综述了 GPS 抗多径干扰的各种定位方法。

关键词：GPS；多径干扰；卫星无线电导航；卫星定位；PN 码测距
中图分类号：V241.6；TN967.1

引　言

随着近距差分 GPS 和民用全球导航卫星系统的发展，选择可用性误差、电离层误差、对流层误差等系统误差都可以进一步消除，动态定位精度已可达亚米级，多径干扰误差变成了主要误差源。由于多径干扰的存在，使基于 GPS 飞机精密进场着陆等高精度应用难以达到指定的精度，克服多径干扰已成为卫星导航研究的热点问题[1~3]。GPS 多径干扰的产生是由于电波从导航星到用户接收机的传播过程中，某些反射体的反射引起，如地面的反射、建筑物或运动载体表面的反射等。接收天线所处的环境不同，建立多径模型也不一样。如对城市街道等复杂环境，可用类似于移动通信衰落信道一样，认为反射分量比较多，接收信号可认为赖思分布。不过报导最多的还是简单一、二径多径模型，这也是分析复杂多径干扰的基础。针对一、二径模型，多数文献只给出的仅仅是在无热噪作用下单独码跟踪环(DLL)的多径跟踪误差，这种方法模型简单，容易得到解析解，但其解仅仅代表 DLL 环静态跟踪偏差。实际上，GPS 接收机采用相干解调技术，而伪距跟踪误差是载波提取环(PLL)和 DLL 环同时作用的结果，客观的假设是 PLL 与 DLL 构成复合环，并在有噪声下研究复合环的跟踪误差。所以本文首先建立多径下这种复合环的等效模型，考虑到这种复合环的数学分析有一定难度，分析了两种特殊情况：(1)通过分析在噪声作用下二阶 DLL 环的跟踪误差特性，研究多径对伪距和伪距变化率误差的均值、方差的影响；(2)在无噪声下研究 PLL 与 DLL 复合环

* 航空科学研究基金(编号：97E52033)和民航自选科技基金资助项目。
收稿日期：1999-09-22；修改稿收到日期：1999-11-20
宋茂忠　男，副教授，1962 年 9 月生。

的跟踪误差，给出多径参数与伪距误差均值的关系，最后综述了GPS抗多径干扰的各种定位方法。

1 多径下伪码跟踪与载波同步复合环的等效模型

GPS接收机主要由两部分组成，一是从天线到中频的前端部分，二是基于大规模集成电路的信号处理部分。信号处理采用可编程的专用芯片，可以12个通道并行工作，每一通道跟踪一颗导航星，由伪码跟踪和载波同步复合环测得伪距和载波相位，复合环如图1所示。

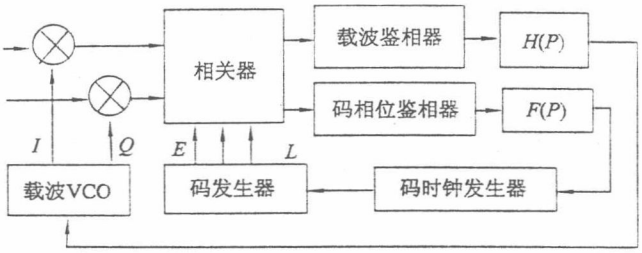

图1 伪码跟踪和载波同步复合环模型

考虑到GPS信号码分多星的正交性，只需分析一颗星的信号。若接收天线附近有电波反射体，则接收到来自某一颗星信号除直达分量外，还有许多多径分量，其归一化中频信号为

$$S_{if}(t) = C[t - T(t)]\exp[-\mathrm{j}(W_{if}t + Q_0) + \sum_{m=1}^{N} A_m C[t - T(t) - D_m]\exp[-\mathrm{j}(W_{if}t + Q_0 + B_m)] + K_s n_1(t) \quad (1)$$

式中：$C(t)$是C/A码序列，$T(t)$为伪距对应的时延值，W_{if}是中频角频率，Q_0是直射信号相位，A_m，D_m，B_m分别为第m个多径信号的振幅、时延和相位延迟量

$$B_m = W_c D_m + Q_m \quad (2)$$

W_c为L_1信号的载波角频率，Q_m是由于反射和天线等引起的第m径反射信号相对于直射信号的传播附加相差(详见第2部分讨论)。K_s是直射信号电平的倒数。

若本地载波环和码跟踪环都处于锁定状态，相位跟踪误差为B_e，归一化码环跟踪误差为E_e

$$B_e = B_0(t) - B_v(t) \quad (3)$$

$$E_e = (1/T_c)[T(t) - T_v(t)] \quad (4)$$

式中：T_c为C/A码码元宽度，$B_0(t)$为实际相位，$B_v(t)$为估计相位，$T_v(t)$为估计伪距。根据图1的框图不难导出复合环的跟踪误差量满足如下微分方程

$$\mathrm{d}E_e/\mathrm{d}t = (1/T_c)\mathrm{d}T/\mathrm{d}t - F(P)[S(E_e, B_e) + K_s n_2(t)] \quad (5)$$

$$\mathrm{d}B_e/\mathrm{d}t = \mathrm{d}B_0/\mathrm{d}t - H(P)U(E_e, B_e) \quad (6)$$

式中：$n_2(t)$为DLL环的等效噪声，$F(P)$和$H(P)$为对应滤波器的传递函数。$S(E_e, B_e)$为多径下DLL的等效S曲线函数

$$S(E_e, B_e) = S_0(E_e)\cos(B_e) + \sum_{m=1}^{N} A_m S_0(E_e - D_m/T_c)\cos[B_m + B_e] \quad (7)$$

$S_0(x)$为无多径时的 S 曲线函数,对全时间 DLL,$S_0(E_e)=R(E_e-1/2)-R(E_e+1/2)$,$R(x)$是归一化 C/A 码自相关函数。对数字锁相环(DPLL),若采用主值在[0,2π]的 arctan 函数,其鉴相特性 $e(t)=\arctan(Q(t)/I(t))$,$e(t)$在第几象限由 $Q(t)$和 $I(t)$的符号决定,即数字锁相环(DPLL)的等效鉴相特性函数 $U(E_e,B_e)$为

$$U(E_e,B_e)=\arctan[Q(t)/I(t)] \tag{8}$$

$$I(t)=R(E_e)\cos(B_e)+\sum_{m=1}^{N}A_mR(E_e-D_m/T_c)]\cos[B_m+B_e]+K_an_c \tag{9}$$

$$Q(t)=R(E_e)\sin(B_e)+\sum_{m=1}^{N}A_mR(E_e-D_m/T_c)]\sin[B_m+B_e]+K_an_c \tag{10}$$

2　多径干扰的电波传播模型

光滑平面和粗糙表面都产生多径,但光滑平面反射信号强,也易于分析。所以下面仅考虑光滑平面反射引入的多径。设直达信号在天线上的电压为

$$S_d(t)=A_0f(e)\exp(\mathrm{j}W_ct-\mathrm{j}g(e)) \tag{11}$$

平面反射产生的第 m 径干扰信号为

$$S_m(t)=AK_mA_0f(\theta)\exp(\mathrm{j}W_ct+2\pi\mathrm{delap}/\lambda-\mathrm{j}B_0-\mathrm{j}g(\theta)) \tag{12}$$

这里 A_0 为信号幅度,AK_m 为平面反射系数,θ 为反射波到达天线时的入射角,λ 为载波的波长,B_0 为平面反射时的相位滞后,$f(x)$和 $g(x)$分别表示接收天线的增益方向图和相位方向图[4],如图 3 所示。如果以直射波的振幅和相位作参考,则考虑到天线后的等效反射系数

$$A_m=AK_mf(\theta)/f(e) \tag{13}$$

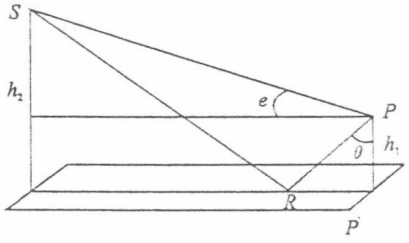

图 2　多径反射几何视图

等效相位滞后量

$$B_m=2\pi\mathrm{delap}/\lambda+B_0+(g(\theta)-g(e)) \tag{14}$$

为了分析反射信号的参数,考虑如下几何模型(见图 2)。

模型以反射平面为基准面,接收天线 P 到基准面的距离为 h_1,卫星 S 到基准面的距离为 h_2,卫星到天线的视线 SP 与基准面的夹角为视线仰角 e。根据光学反射原理,反射电波路径 $SR+RP$ 与直射电波 SP 的路径之差

$$\mathrm{delap}=\sqrt{4h_1*SP*\sin(e)+SP*SP+4h_1h_1}-SP \tag{15}$$

因 $h_1\ll SP$,所以 $\mathrm{delap}\approx 2h_1\sin(e)$,而反射波的入射角 $\theta=\angle RPP'$

$$\sin(\theta)=\frac{SP*\cos(e)}{SP+2h_1*\sin(e)} \tag{16}$$

3　无噪声下多径参量对复合环伪距误差的影响

无噪声下多径干扰对伪距误差的影响就是求解码跟踪环 DLL 与载波环 PLL 复合环的稳态解。对非线性随机微分方组(5,6),为简单起见,不防设两个子环都是一阶环路,$F(P)=$